Electronic Supplementary Material (ESI) for Journal of Materials Chemistry C.

SUPPORTING INFORMATION FOR:

Polymorphism in N,N'-dialkyl-naphthalene diimides

Silvia Milita, Fabiola Liscio, Lewis Cowen, Massimiliano Cavallini, Ben A.Drain, Thibault Degoussée, Sally Luong, Oliver Fenwick, Antonietta Guagliardi, Bob C. Schroeder, Norberto Masciocchi**

Figure S1: NMR spectra in $CDCl_3$ solution of a) NDI4, b) NDI6, c) NDI8 and d) NDI10.

Figure S2: Normalized UV-vis absorption spectra of all NDI derivatives in $CDCl_3$ solution.

Supplementary Text: Crystal structure solution from laboratory XRPD data, including **Figure S3**.

Supplementary Text: Cell determination (indexing) of the 6β, 6γ and 6δ crystal phases.

Supplementary Text: Crystal structure solution of the 6γ phase from laboratory XRPD data, including **Figure S4** (Rietveld refinement plot for 6γ phase) and **Figure S5** (molecular structure and conformation of NDI6 in the 6γ phase).

Figure S6: The colours of the powders of the pristine NDIx a-phases (left to right: x = 4, 6, 8, 10).

Supplementary Text: AFM of NDI6 and NDI8 thin films, including **Figure S7.**

Figure S8: Experimental GIXRD images and specular scans of NDI4 (a, e), NDI6 (b, f) NDI8 (c, g) and NDI10 (d, h) films.

Figure S9: 2D-GIXRD image of NDI6 and the calculated positions of Bragg peaks from the simulated structure. Only the-indices of the most intense spots are reported.

Figure S10: POM of NDI6 powder recorded during the first cooling process from the melt: a) 200, b) 155 and c) 55°C.

Figure S11: a) 2D-GIXRD image and b) specular XRD profile of NDI6 drop-casted film.

Figure S12: Specular XRD patterns of NDI6 film at RT (black) and at 100°C (red).

Supplementary Text: Specular XRD *in situ* measurements of NDI6 thin film.

Figure S13: Specular XRD patterns of NDI6 film at RT at 100°C recorded every 30 minutes.

Figure S14: Specular XRD patterns of NDI6 film recorded at RT as deposited (black curve) and at different times after the thermal treatment at 100°C: after 1.5 hours (green curve), after 6 days (pink curve) and after 24 days (purple curve).

Figure S15: OM images of drop cast NDI6 film recorded at r.t., 60°C and 180°C with polarized light (top) and in bright field (bottom).

Figure S16. The full DSC traces for two heating/cooling cycles of NDIx (x =4,6,8,10) species.

Table 1. A summary of the transition temperatures (°C) and enthapies (kJ mol^{-1}) for the NDIx (x = 4, 6, 8 and 10) species.

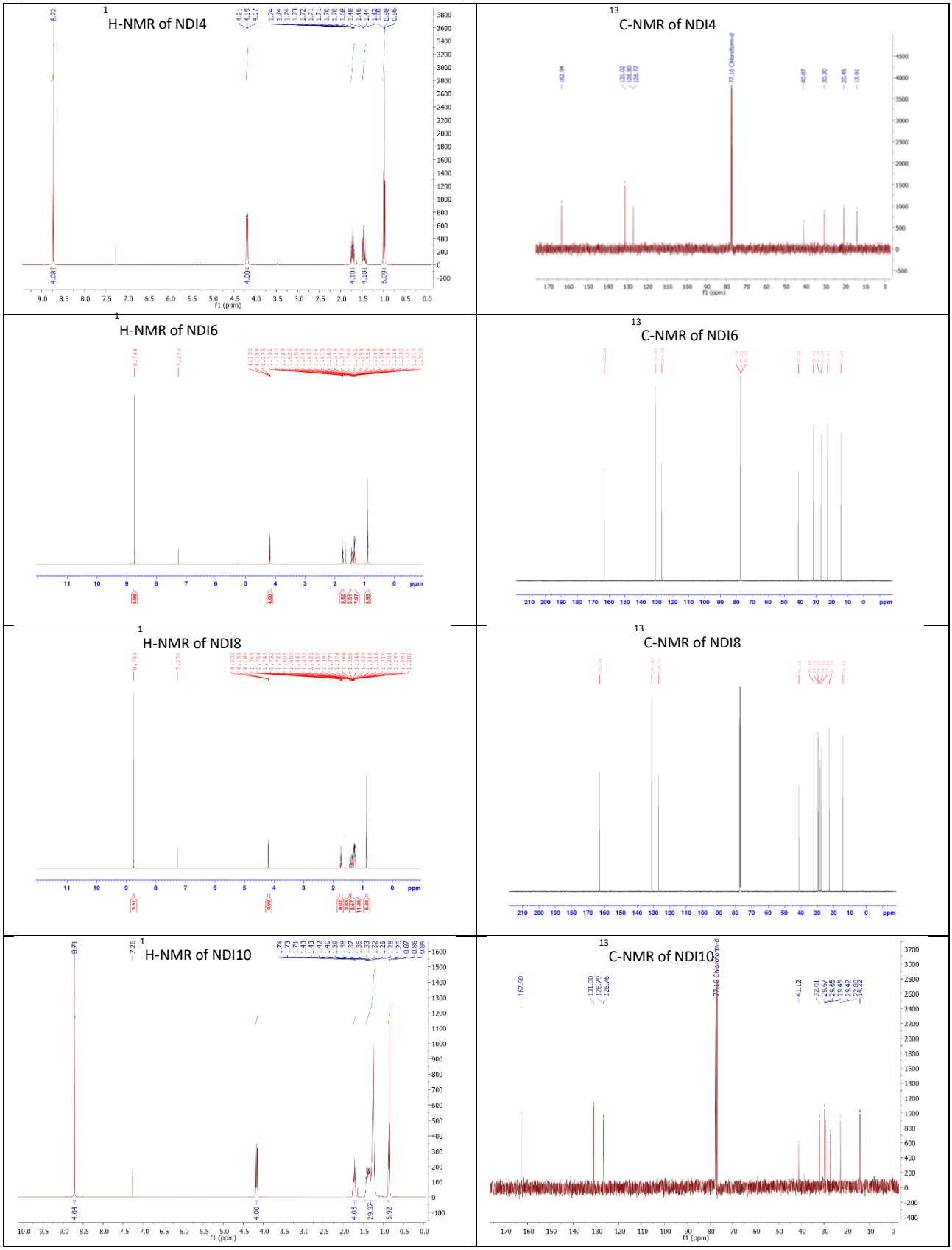

Figure S1: : NMR spectra in $CDCl_3$ solution of a) NDI4, b) NDI6, c) NDI8 and d) NDI10.

^{1}H-NMR of NDI4

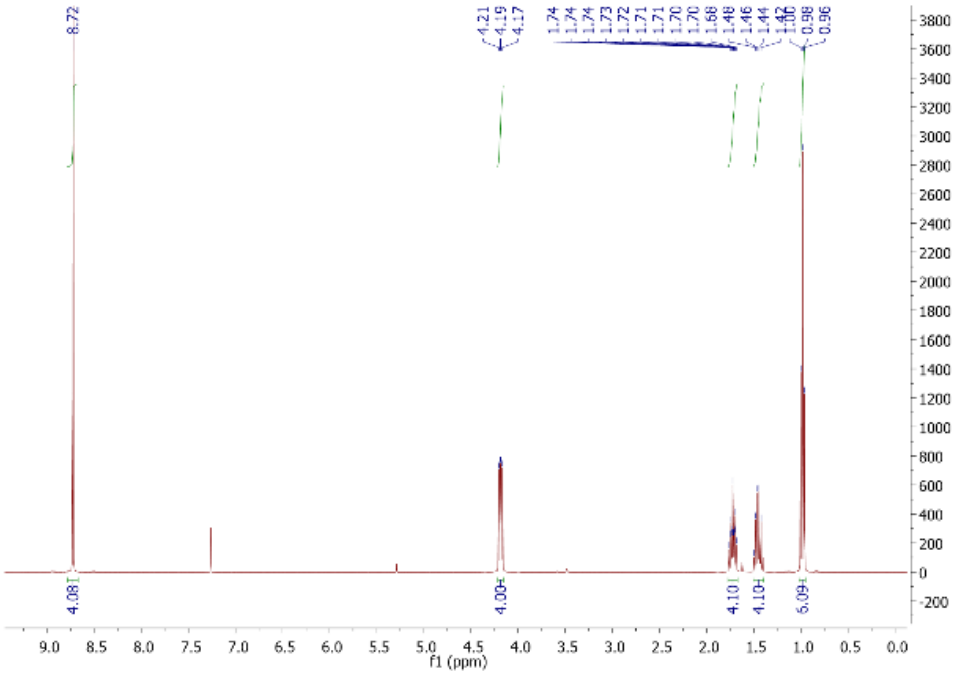

^{13}C-NMR of NDI4

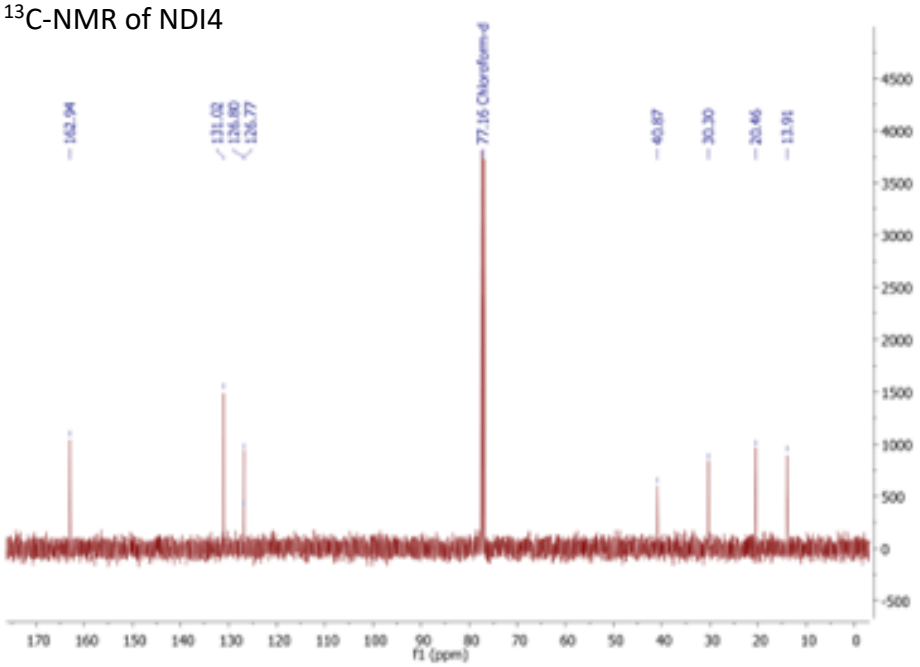

Figure S1a: NMR spectra in $CDCl_3$ solution of NDI4 (magnified).

^{1}H-NMR of NDI6

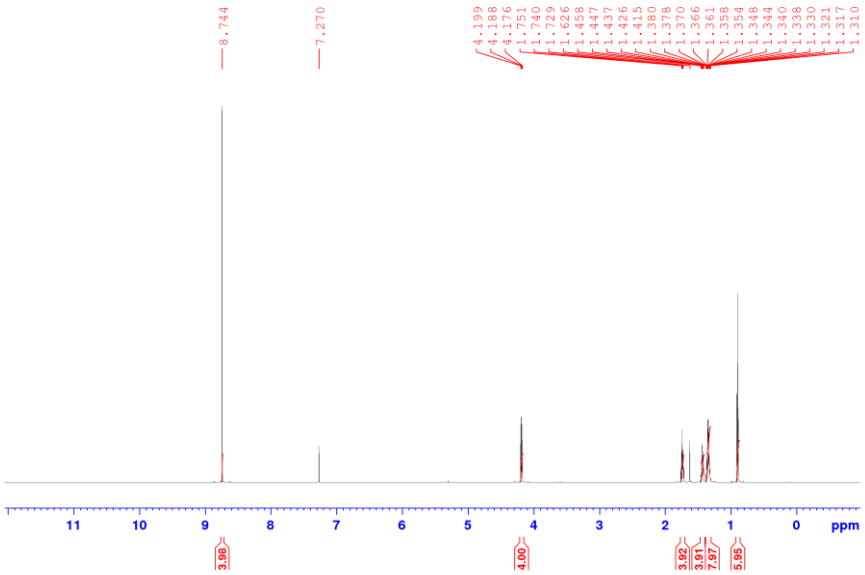

^{13}C-NMR of NDI6

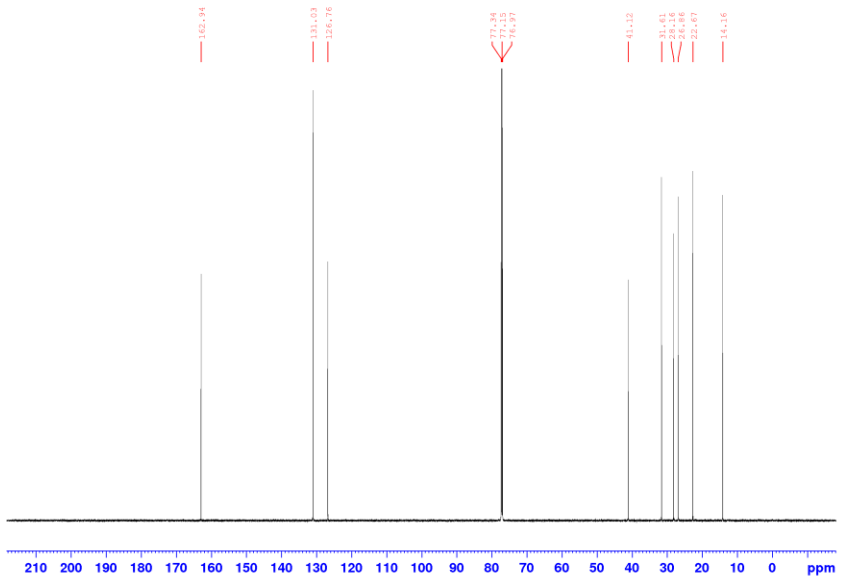

Figure S1b: NMR spectra in $CDCl_3$ solution of NDI6 (magnified).

^{1}H-NMR of NDI8

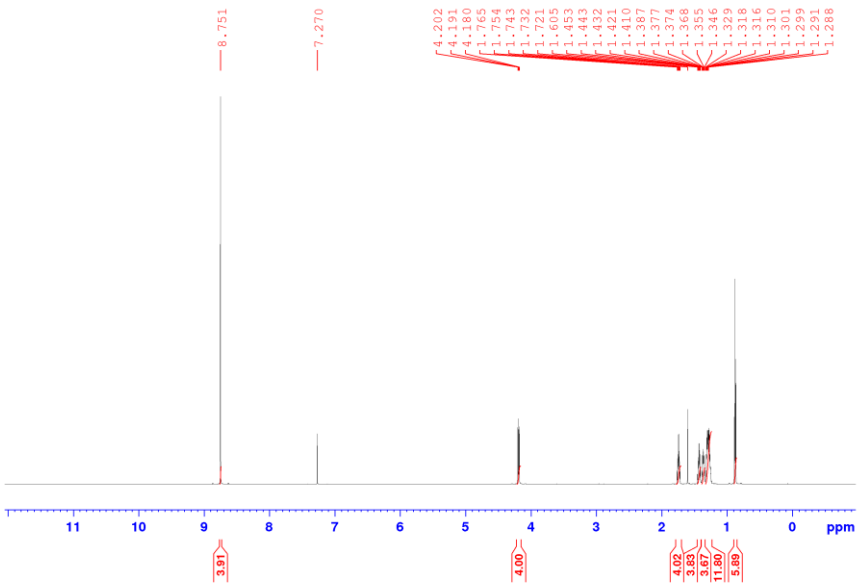

^{13}C-NMR of NDI8

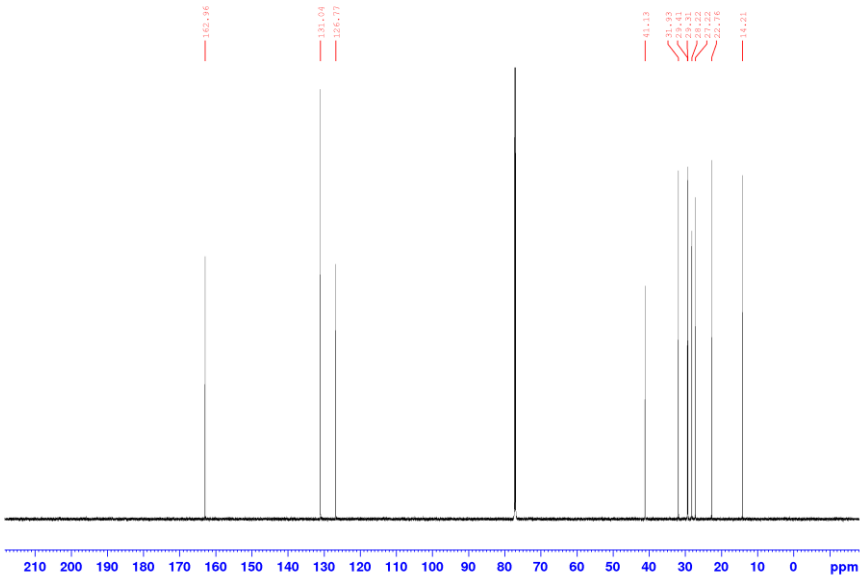

Figure S1c: NMR spectra in $CDCl_3$ solution of NDI8 (magnified).

^{1}H-NMR of NDI10

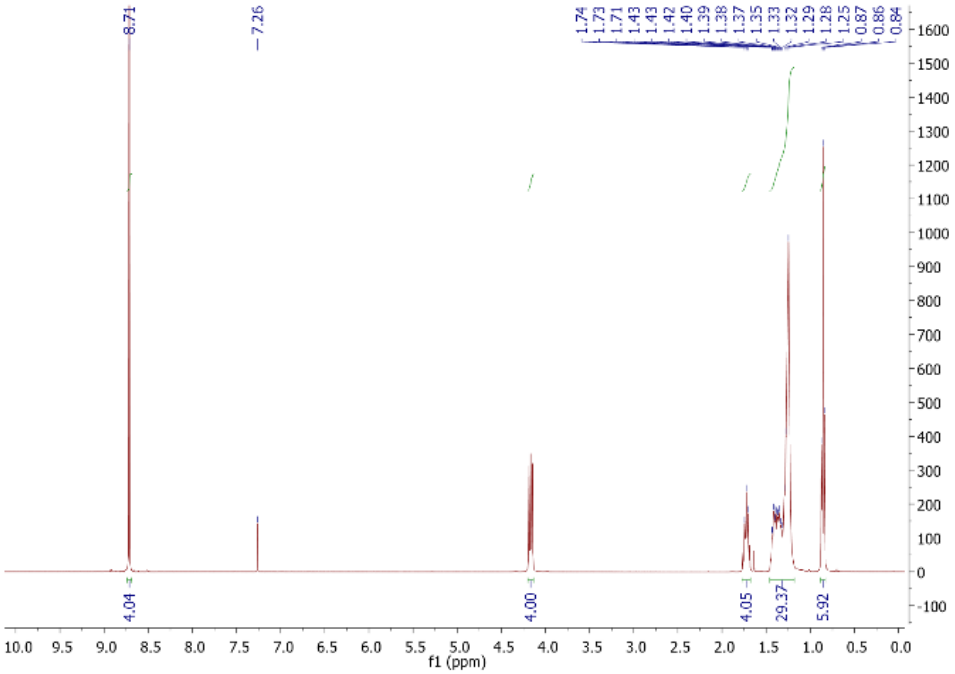

^{13}C-NMR of NDI10

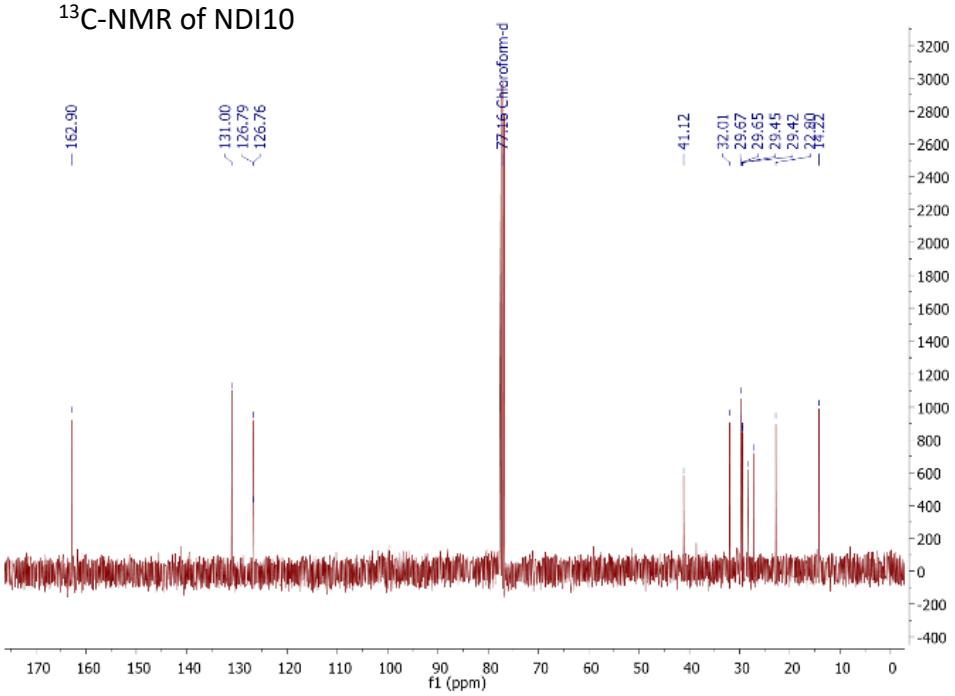

Figure S1d: NMR spectra in $CDCl_3$ solution of NDI10 (magnified).

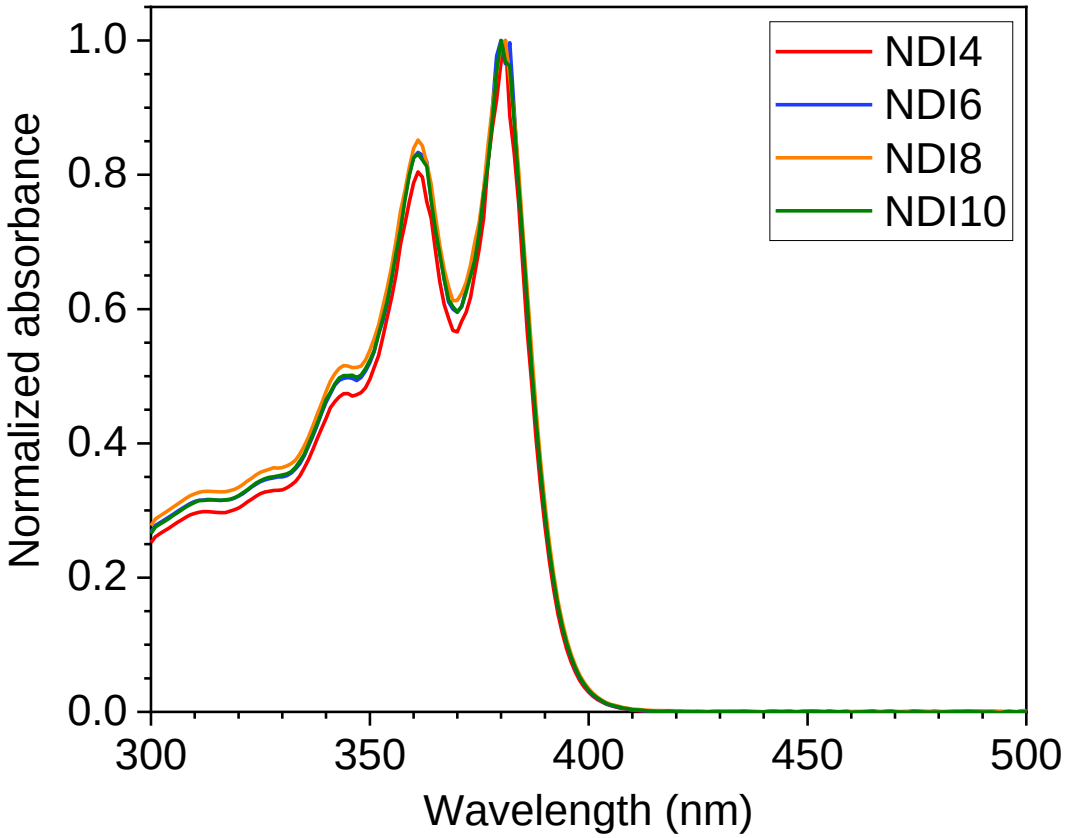

Figure S2: Normalized UV-vis absorption spectra of NDIx (x = 4,6,8,10) derivatives in $CHCl_3$ solution.[1]

Supplementary Text: Crystal structure solution from laboratory XRPD data.

Diffraction data for structure solution of the 8α and 10α phases were collected in the 2-92° 2θ range, sampling at 0.02°, with scan time lasting approximately 16 h. Standard peak search methods, followed by profile fitting, allowed the accurate estimate of the low-angle peak position, which, though the SVD indexing algorithm[2] implemented in TOPAS-R[3] provided triclinic cells with GOF(20) = 31.8 and 33.8[4], for 8α and 10α, respectively. Density considerations clearly indicated Z = 1 for both phases, with NDI8 and NDI10 molecules lying on an inversion centre.

Structure solutions were performed by Monte Carlo / Simulated Annealing technique[5] using a rigid model, flexible about the alkylic C-C bonds and the Z-matrix formalism with standard geometrical parameters for covalently bonded atoms. The final refinements were eventually carried out by the Rietveld method, maintaining the rigid bodies introduced at the structure solution stage. The background was modelled by a polynomial function of the Chebyshev type, peak profiles were described by the Fundamental Parameters Approach[6] and a common (refinable) isotropic thermal factor was attributed to all atoms. A second-order spherical harmonics description of the lorentzian peak broadening caused by anisotropic crystal size effects was also necessary, together with a significant correction for preferred orientation effects, with (100) and (001) poles, for 8α and 10α, respectively. The final Rietveld refinements plots for the 8α and 10α phases are shown in Figure S3. Fractional atomic coordinates and crystal structure details were deposited with the CCDC (CSD Codes 1972223 and 1972224). These data can be obtained free of charge upon request from the Cambridge Crystallographic Data Centre via www.ccdc.cam.ac.uk/data_request/cif.

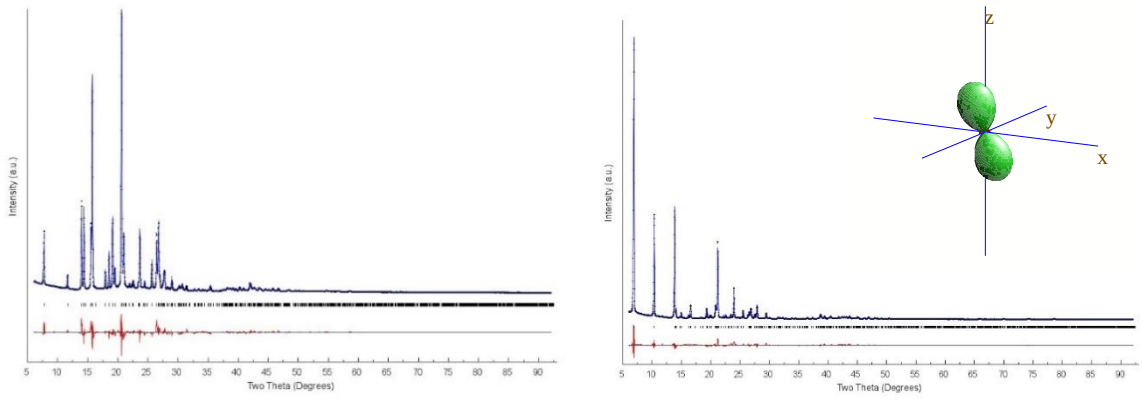

Figure S3. Final Rietveld refinement plots for 8α (top) and 10α (bottom), with difference plot and peak tick-marks at the bottom. In both cases, the strongest peak, falling at 2θ < 4°, dominating the entire XRPD pattern, has been eliminated. The inset in the right panel addresses pictorially shows the deformation tensor calculated by comparing iso-oriented unit cells of 8α and 10α, highlighting in green the large variation occurring along one single axis (here, **c**) and nearly null modification normal to it (the tiny, barely visible, negative lobes, in red).

Supplementary Text: Cell determination (indexing) of the 6β, 6γ and 6δ crystal phases.

The XRPD data of these elusive crystal phases were of significantly poorer quality than the pristine diffraction data obtained on pure (as crystallized) 6α. Consequently, it was only possible to assess the lattice metrics, and the probpable space group symmetry, by selectively discriminating, among the proposed indexing solutions, the most plausible ones, ranked by the goodness of fit of the "selectively chosen" diffraction peaks (i.e. taking care of the possibility of residual signals from contaminant, not fully transformed, phases – attributed to thermal gradients or heavy hysteretical effects).

The table below summarizes the results from indexing (performed using the SVD procedure[2] procedure implemented in the TOPAS-R program,[3] similarly as described for 6α in a previous section).

Crystal phase	a, Å	b, Å	c, Å	α, °	β, °	γ, °	V, Å^3	Z	GOF	Number of peaks	$2\theta_{max}$
6β	22.84	4.85	32.06	90	91.9	90	3552	6	13.0	36	21.3
6γ[a]	4.89	6.49	20.95	73.1	80.3	75.9	611	1	15.1	26	30.1
6δ	8.83	37.96	8.03	90	84.8	90	2685	4	10.0	36	27.7

[a] The reduced cell for 6γ is: a = 4.89, b = 6.49, c= 20.05, α = 91.2, β = 95.6, γ = 104.1°.

From these values, it is manifestly evident that the (way too) large unit cell of the 6β phase hampers a meaningful structural determination of the molecular arrangement and its crystal packing. Similar considerations partially hold for 6δ, the highest-temperature crystal phase, stable only near 200°C. Consequently, only the new crystal structure of the 6γ phase is here tentatively presented, and discussed in the following section.

Supplementary Text: Crystal structure solution of the 6γ phase from laboratory XRPD data.

Powders of the 6γ phase, obtained *in situ* by cooling from the 6δ phase down to 100°C (before 6β appears), using a simple heating stage (operating in air and electronically controlled by a device assembled by Officina Elettrotecnica di Tenno, Italy), provides a XRPD trace, indexed by the triclinic cell shown above. Crystal structure solution and refinement were performed as described above for species 8α and 10α, and resulted in the final Rietveld Refinement plot shown below. Obviously, the quality of the data and the paucity of the corresponding Bragg peaks (larger 2θ angles being almost unaccessible in this setup), make the crystal structure model of much lower quality than desirable. Nevertheless, poor(er) information in better than no infomation at all.

*Crystal data for **6γ (NDI6 γ-phase)***: $C_{26}H_{30}N_2O_4$, fw = 434.54 g mol^{-1}, triclinic P-1, a = 4.9025(5) , b = 6.4989(8) , c = 20.946(3) Å, α = 73.15(1), β = 80.29(1), γ = 75.862(8) °, V = 615.9(1) Å^3, Z = 1, ρ_{calc} = 1.172 g cm^{-3}, μ(Cu-Kα) = 6.4 cm^{-1}, R_p and R_{wp}, 0.037 and 0.053 respectively, for 1201 data collected in the 4-28° 2θ range. R_{Bragg} = 0.017.

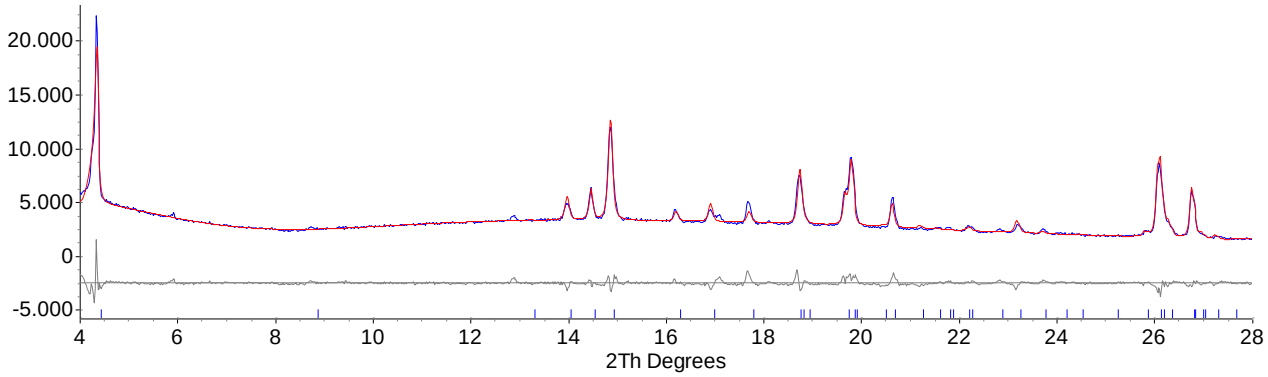

Figure S4. Final Rietveld refinement plot for 6γ crystal phase, measured at 100°C. Blue trace: observed data; red trace: calculated data; grey trace: the difference plot. Blue markers at the bottom: calculated peak positions.

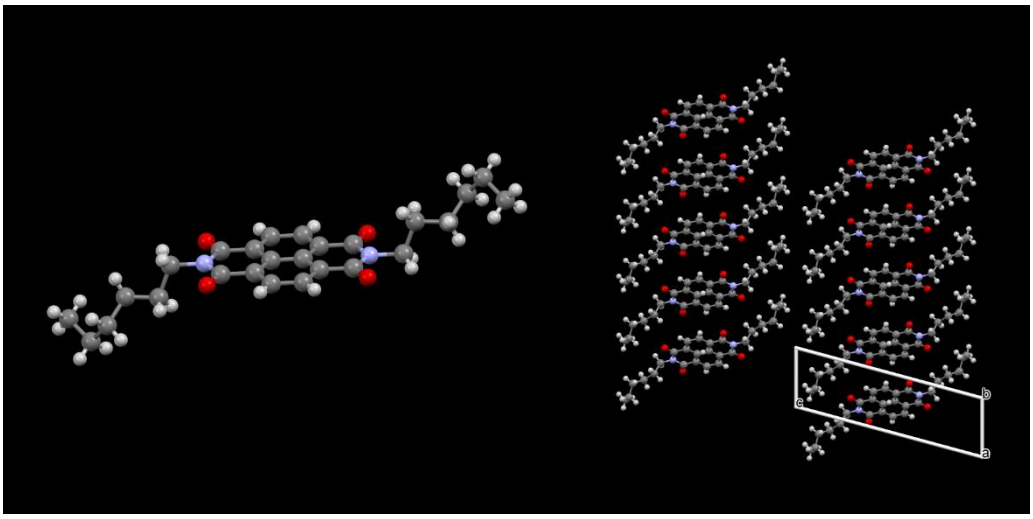

Figure S5. Left: Molecular structure and conformation of NDI6 in the 6γ phase. Right: a sketch of the crystal packing of 6γ at 100°C, viewed down [100].

Figure S6: The colours of the powders of the pristine NDIx α-phases (left to right: x = 4, 6, 8, 10).

Supplementary Text: Atomic force microscopy of NDI6 and NDI8 thin films

Thin films of NDI6 and NDI8 were spin-coated on glass substrates at 800 RPM for 3s (reached in 0.1s) then 2000 RPM for 20s (reached in 0.2s). The films were then annealed at 80°C for 15 minutes.

NDI6: Two separate films were kept at RT or at 120°C on a hot-plate, in air, for 25 minutes. The heated film was then removed from the hot plate and imaged while cooling down (Figure S7a, second image). The film was then allowed to fully cool down to room temperature (by leaving it at RT for 2 hours), prior imaging the films again (Figure S7a, third image). AFM images cannot be used to unambiguously identify crystal phases, so here we attempt to correlate morphological changes observed by AFM to the crystal phases observed by XRD in the main text. Pristine thin film of NDI6 at RT consists on crystals several micrometers long together with small aggregates. These two crystal types could correspond to the 6α and 6β phases shown by XRD. After heating to 120°C, the large crystallites become connected, and increase in size and flatness. The changes are compatible to a molecular rearrangement in another phase, i.e. the 6γ phase. On the other hand, the small aggregates are still uniformly distributed between the crystals. Upon fully cooling back to RT (Figure S7a, third image)., the film keeps the morphology adopted upon heating (Figure S7a, second image). Indeed, the XRD data indicated that the 6γ $\rightarrow$6β transition takes days to complete (main text), which explains the invariance of the topography taken after only 2 hours of cooling,

NDI8: The topography of NDI8 thin film clearly shows the stacking of molecular layers in a terraced morphology (Figure S6b). The height changes have been numbered along the profile line (green dash line on Figure S6b) and they well correspond to the stacking observed by XRD (see main text).

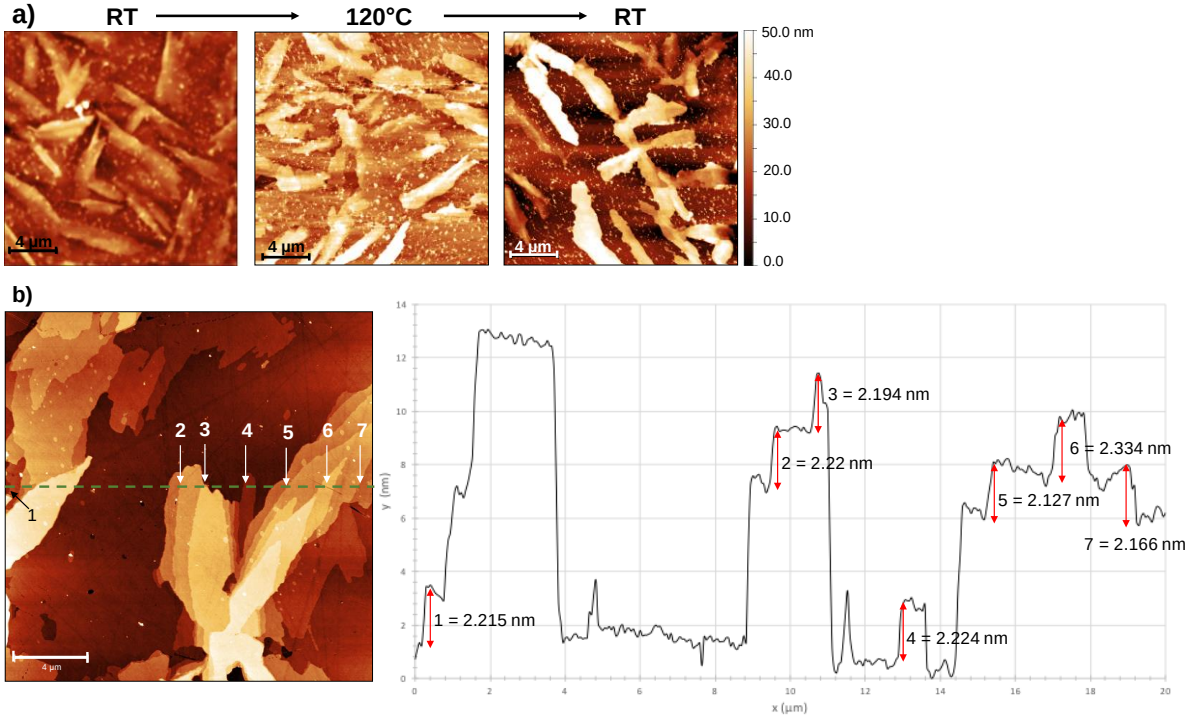

Figure S7: AFM analysis of a) thin films of NDI6 immediately after heating to specified temperature and after cooling back to RT; b) thin film of NDI8 showing the stacking of the molecules.

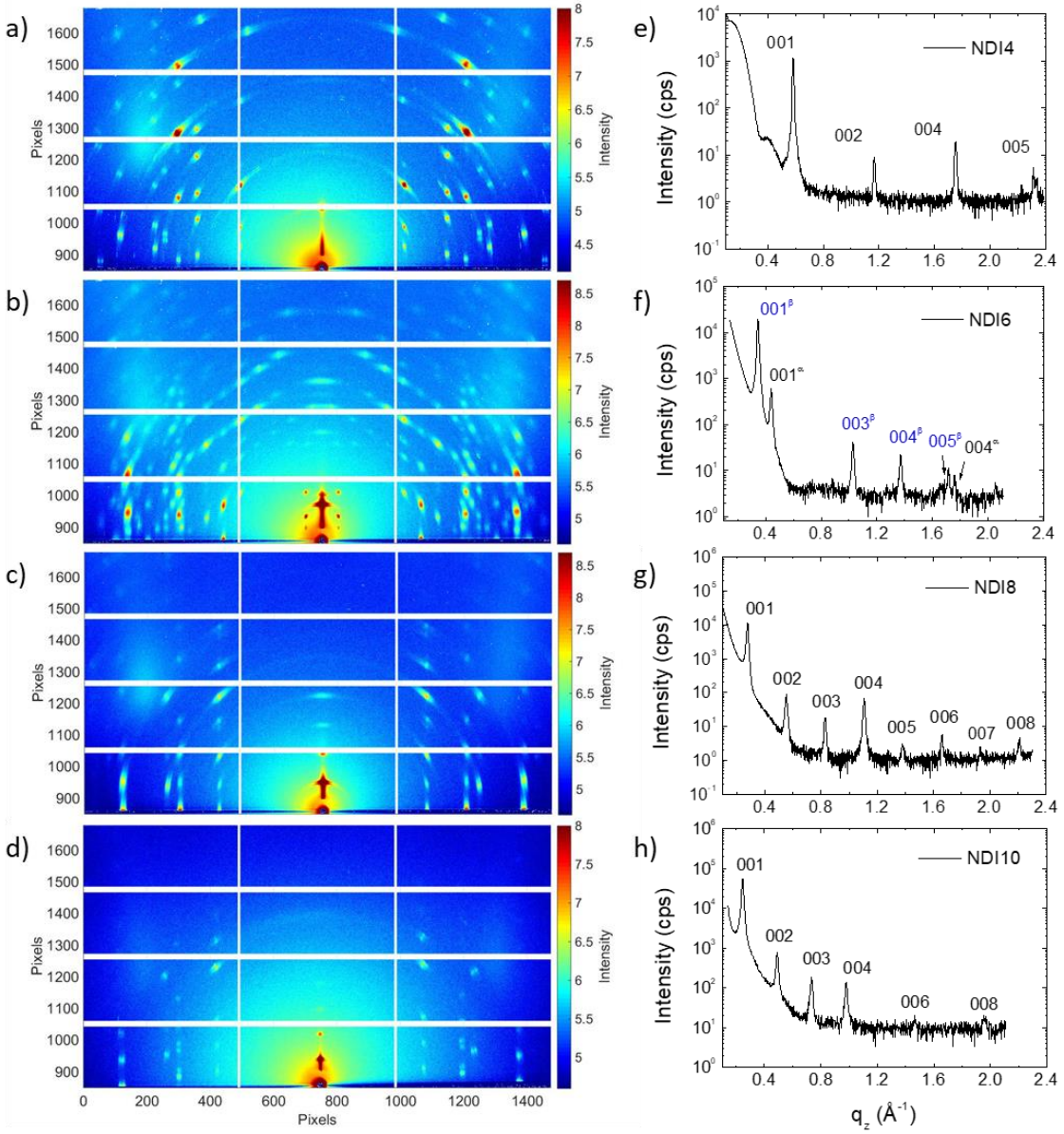

Figure S8: Experimental GIXRD images and specular scans of NDI4 (a, e), NDI6 (b, f) NDI8 (c, g) and NDI10 (d, h) films.

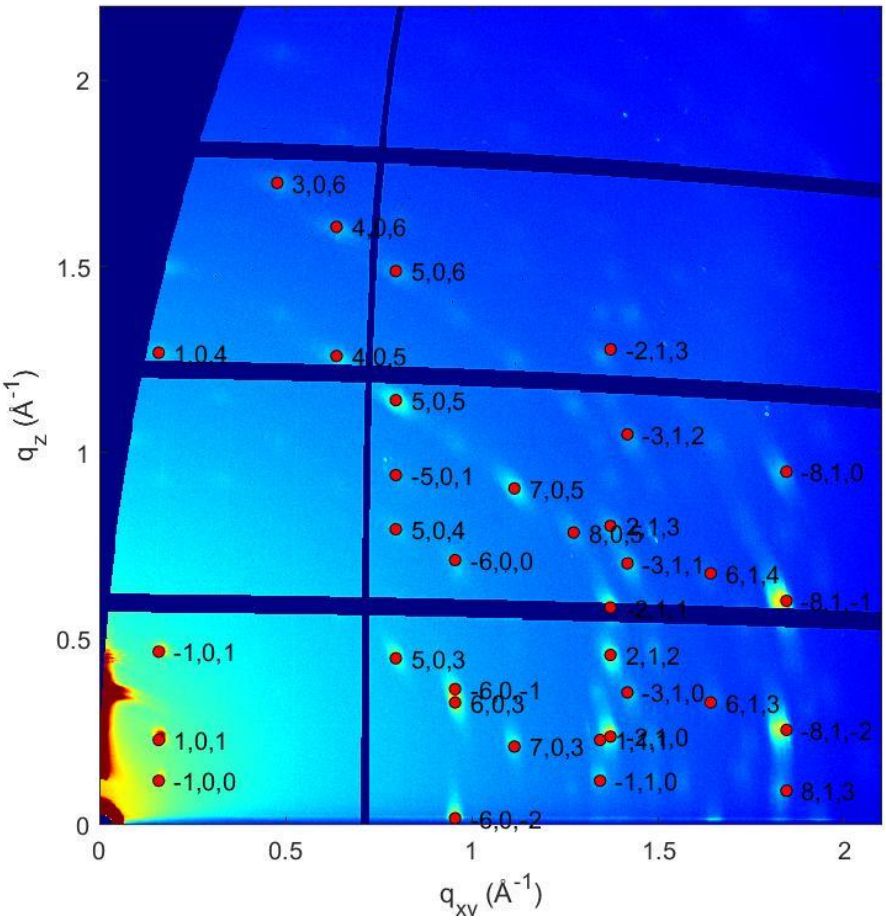

Figure S9: 2D-GIXRD image of a NDI6 film (6β phase) and the calculated positions of Bragg peaks from the simulated structure. Only the indices of the most intense spots are reported. Indices refer to the unit cell in conventional setting (see main text, section Results and Discussion: (c) Structure of the films).

The evolution of POM images collected upon cooling NDI6 from the melt shows several phase transformations (also identified by DSC and thermodiffractometry): a) at 200°C, a continous crystalline film forms, b) at 155°C, cracks and/or fibers appear (corresponding to δ to γ transition) and c) the crystalline fiber colour changes at 55°C (corresponding to the γ to $\alpha+\beta$ transition).

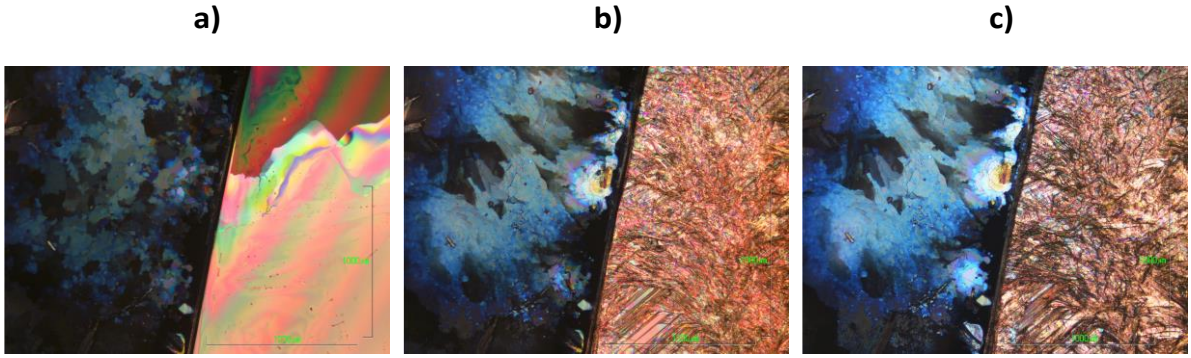

Figure S10: POM of NDI6 powder recorded during the first cooling process from the melt: a) 200, b) 155 and c) 55°C.

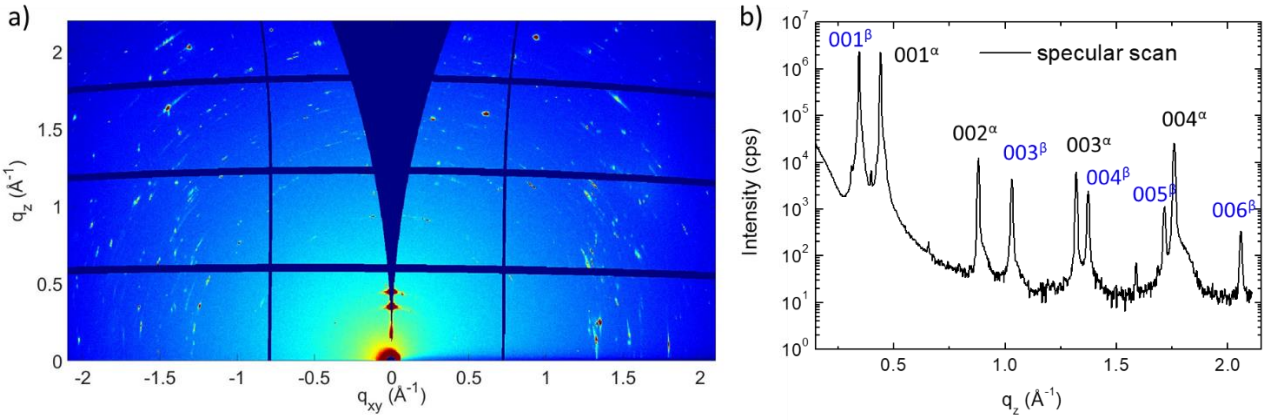

Figure S11: a) 2D-GIXRD image and b) specular XRD profile of NDI6 drop-casted film.

Supplementary Text: Specular XRD *in situ* measurements of NDI6 thin film

We performed *in situ* XRD measurements in specular geometry during the thermal annealing at 100°C. Figure S12 compares the data recorded at RT and at 100°C. The pristine NDI6 film consists of a mixture of 6α and 6β phases, the latter being largely the dominant one. When annealed at 100°C, the 6*β phase* disappears, forming the 6*γ phase*, whereas the 6*α phase* persists (with a slight thermal expansion). The phase transition occurs within few minutes and the crystal structure does not change after annealing the sample for two hours at 100 °C, as evidenced by the constancy of the subsequent specular XRD patterns, each one lasting 30 minutes (Figure S13).

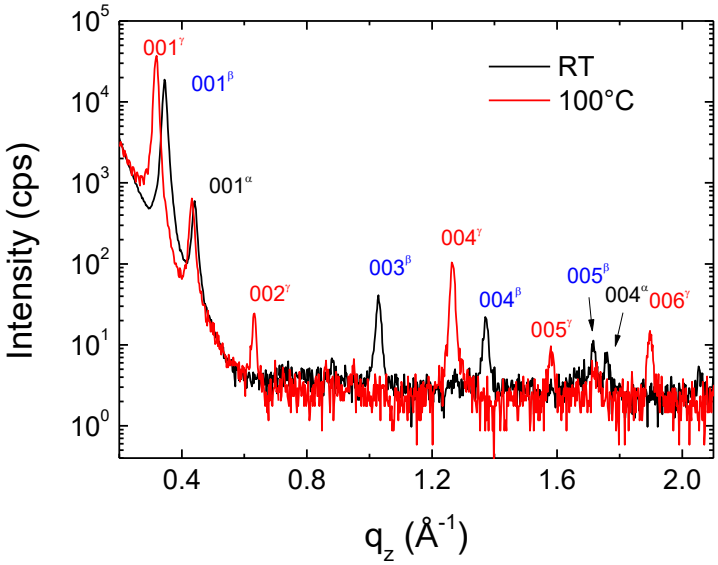

Figure S12: Specular XRD patterns of NDI6 film at RT (black) and at 100°C (red).

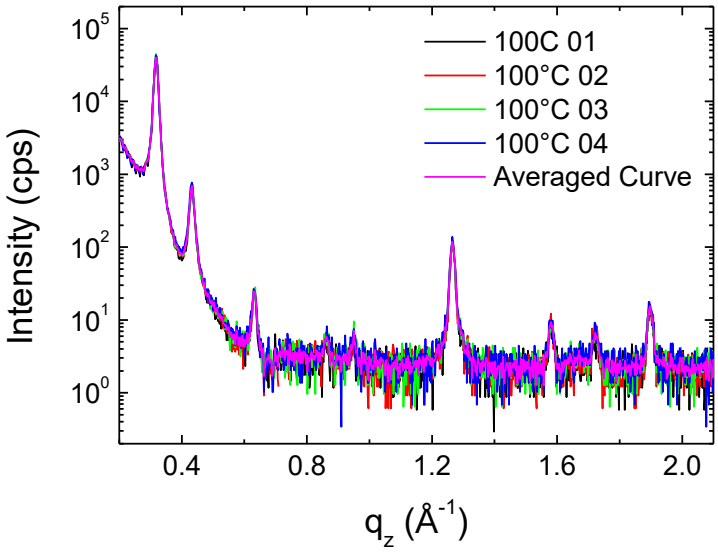

Figure S13: Specular XRD patterns of NDI6 film at RT at 100°C recorded every 30 minutes.

When cooled to RT, the NDI6 film did not recover the pristine structure and 6γ phase is still present after 1.5 hours, the reverse γ to β phase transition being kinetically inhibited. Indeed, an XRD measurement, recorded after 24 days, shows still the presence of a significant amount of β phase (peak at *ca*. 0.35 $Å^{-1}$, Figure S14).

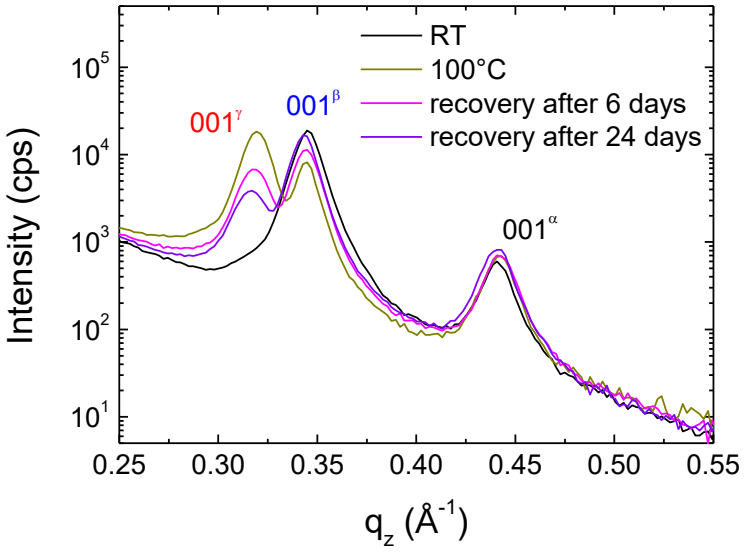

Figure S14: Specular XRD patterns of NDI6 film recorded at RT as deposited (black curve) and at different times after the thermal treatment at 100°C: after 1.5 hours (green), after 6 days (pink) and after 24 days (purple).

The phase transformations of a drop-casted NDI6 film upon heating are evidenced by the evolution of the OM images collected by using polarized light and under bright field conditions. The images do not change from RT up to 60°C where the appearance of straight lines, highlighted by arrows, indicates the occurrence of the β to γ transition, followed by a more extended change (crystal fragmentation) at 180 °C, corresponding to the γ to δ transition.

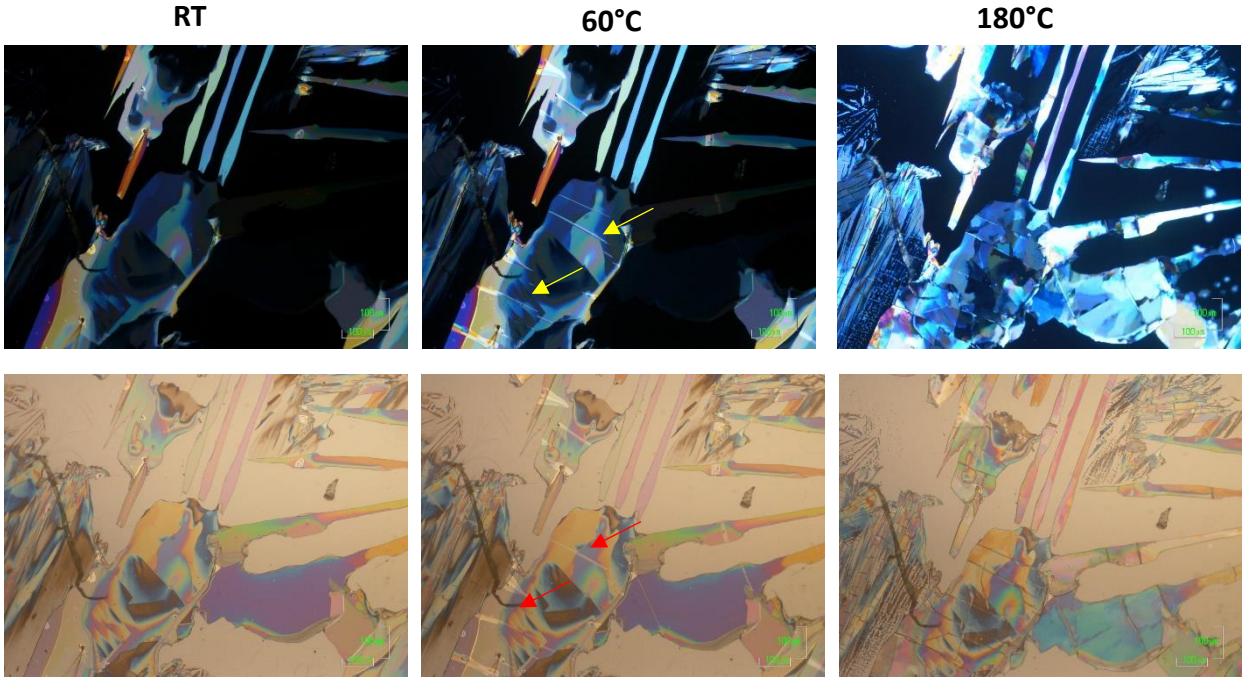

Figure S15: OM images of a drop-casted NDI6 film recorded at RT, 60 °C and 180 °C with polarized light (top) and in bright field (bottom).

Table S1. A summary of the transition temperatures (°C) and enthapies (kJ mol^{-1}) for the NDIx (x = 4, 6, 8 and 10) species. Italicized items indicate broad, and difficult to detect, thermal events. Only the **first** heating and cooling cycle values are here reported.

	NDI4 on heating	NDI4 on cooling	NDI6 on heating	NDI6 on cooling	NDI8 on heating	NDI8 on cooling	NDI10 on heating	NDI10 on cooling
T	131.8 4α →4γ	*Very slow transformation to 4α*		49.1 6γ → 6α,6β			163.1 10α → 10β	160.3 10β → 10α
ΔH	18.2	*n.a.*		–5.1			7.3	–7.2
T			178.5 6α → 6γ	148.1 6δ → 6γ				
ΔH			16.5	–13.0				
T	227.2 4γ → LC	169.7 LC → 4γ						
ΔH	3.8	–5.2						
T	234.1 melting	227.5 melt→LC	207.9 melting	200.0 melt→6δ	190.0 melting	185.9 crystallization	180.8 melting	178.2 melt→10γ
ΔH	21.7	–22.2	22.2	–21.1	31.0	–30.7	34.6	–30.2
$\Delta H_{\alpha-melt}$	43.7	n.a.	38.7	–39.2	31.0	c	41.9	–37.4

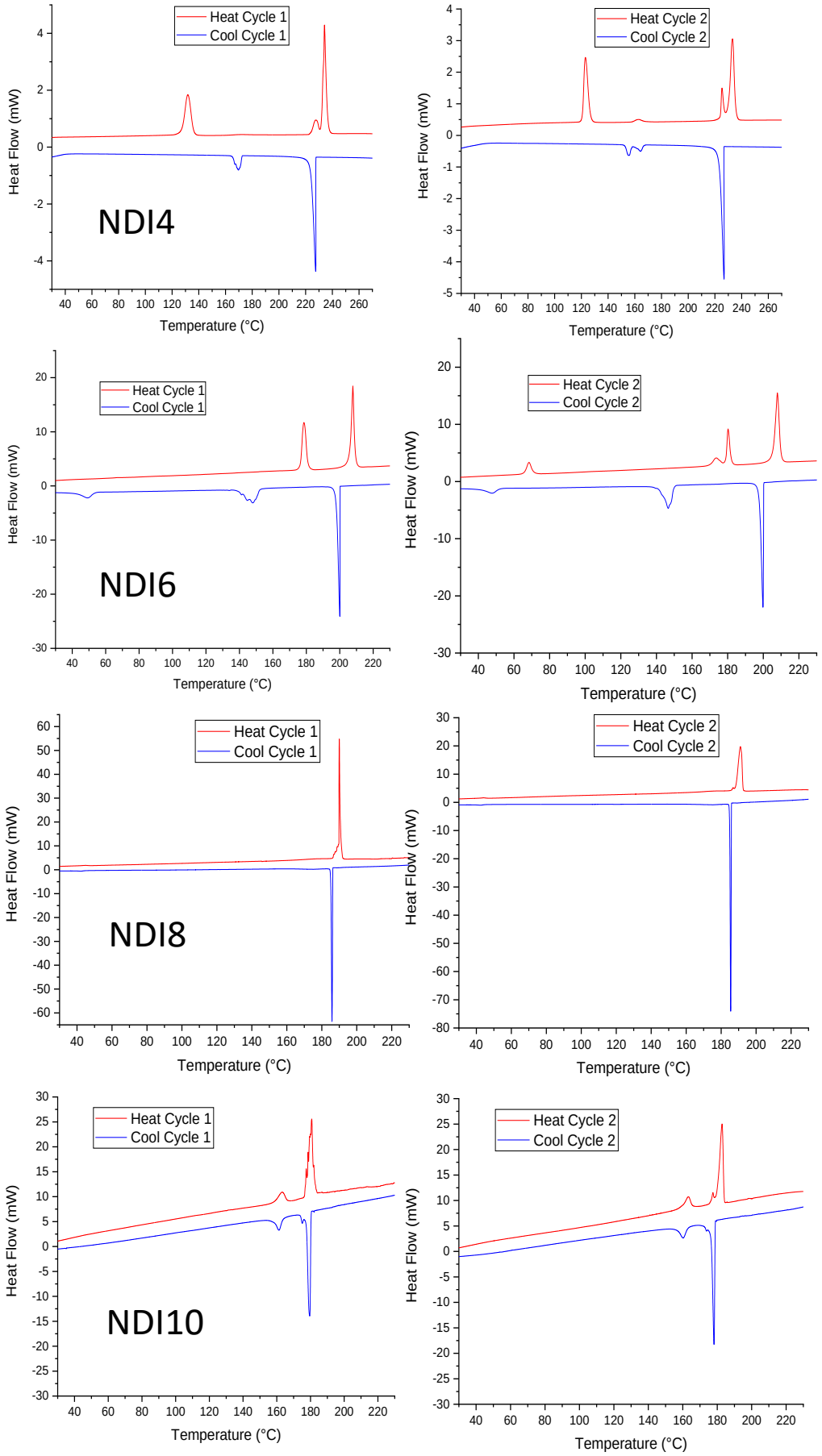

Figure S16. The full DSC traces for two heating/cooling cycles of NDIx (x =4,6,8,10) species.

References

[1] S. V. Bhosale, C. H. Jani and S. J. Langford, *Chem. Soc. Rev*., 2008, **37**, 331–342.
[2] A.A. Coelho, *J. Appl. Cryst.* 2003, **36**, 86-95.
[3] Version 3.0, 2005. Bruker AXS, Karlsruhe (Germany)
[4] G.D. Smith and R.L. Snyder*, J. Appl. Cryst*. 1979, **12**, 60-65.
[5] A.A. Coelho, *J. Appl. Cryst.* 2000, **33**, 899-908.
[6] R.W. Cheary and A.A. Coelho*, J. Appl. Cryst.* 1992, **25**, 109-121.